Bio-Design and Manufacturing (2023) 6:718–734
https://doi.org/10.1007/s42242-023-00250-6

RESEARCH ARTICLE

Accelerated fracture healing by osteogenic Ti45Nb implants through the PI3K–Akt signaling pathway

Jia Tan[1,3] · Jiaxin Li[2] · Zhaoyang Ran[1,3] · Junxiang Wu[1,3] · Dinghao Luo[1,3] · Bojun Cao[1,3] · Liang Deng[1,3] · Xiaoping Li[4] · Wenbo Jiang[3] · Kai Xie[1,3] · Lei Wang[1,3] · Yongqiang Hao[1,3]

Received: 21 December 2022 / Accepted: 8 June 2023 / Published online: 14 September 2023

Abstract

The key to managing fracture is to achieve stable internal fixation, and currently, biologically and mechanically appropriate internal fixation devices are urgently needed. With excellent biocompatibility and corrosion resistance, titanium–niobium alloys have the potential to become a new generation of internal fixation materials for fractures. However, the role and mechanism of titanium–niobium alloys on promoting fracture healing are still undefined. Therefore, in this study, we systematically evaluated the bone-enabling properties of Ti45Nb via in vivo and in vitro experiments. In vitro, we found that Ti45Nb has an excellent ability to promote MC3T3-E1 cell adhesion and proliferation without obvious cytotoxicity. Alkaline phosphatase (ALP) activity and alizarin red staining and semiquantitative analysis showed that Ti45Nb enhanced the osteogenic differentiation of MC3T3-E1 cells compared to the Ti6Al4V control. In the polymerase chain reaction experiment, the expression of osteogenic genes in the Ti45Nb group, such as ALP, osteopontin (OPN), osteocalcin (OCN), type 1 collagen (Col-1) and runt-related transcription factor-2 (Runx2), was significantly higher than that in the control group. Meanwhile, in the western blot experiment, the expression of osteogenic-related proteins in the Ti45Nb group was significantly increased, and the expression of PI3K–Akt-related proteins was also higher, which indicated that Ti45Nb might promote fracture healing by activating the PI3K–Akt signaling pathway. In vivo, we found that Ti45Nb implants accelerated fracture healing compared to Ti6Al4V, and the biosafety of Ti45Nb was confirmed by histological evaluation. Furthermore, immunohistochemical staining confirmed that Ti45Nb may promote osteogenesis by upregulating the PI3K/Akt signaling pathway. Our study demonstrated that Ti45Nb exerts an excellent ability to promote fracture healing as well as enhance osteoblast differentiation by activating the PI3K/Akt signaling pathway, and its good biosafety has been confirmed, which indicates its clinical translation potential.

Jia Tan, Jiaxin Li, and Zhaoyang Ran have contributed equally to this work.

✉ Kai Xie
kai.xie@hotmail.com

✉ Lei Wang
wanglei12041985@163.com

✉ Yongqiang Hao
hyq_9hospital@hotmail.com

[1] Shanghai Key Laboratory of Orthopaedic Implants, Department of Orthopaedic Surgery, Shanghai Ninth People's Hospital, Shanghai Jiao Tong University School of Medicine, Shanghai 200011, China

[2] Department of Orthopedics, The Second Affiliated Hospital of Harbin Medical University, Harbin 150001, China

[3] Clinical and Translational Research Center for 3D Printing Technology, Shanghai Ninth People's Hospital, Shanghai Jiao Tong University School of Medicine, Shanghai 200011, China

[4] Ningxia Orient Ta Ind Co., Ltd., Shizuishan 753000, China

Graphic abstract

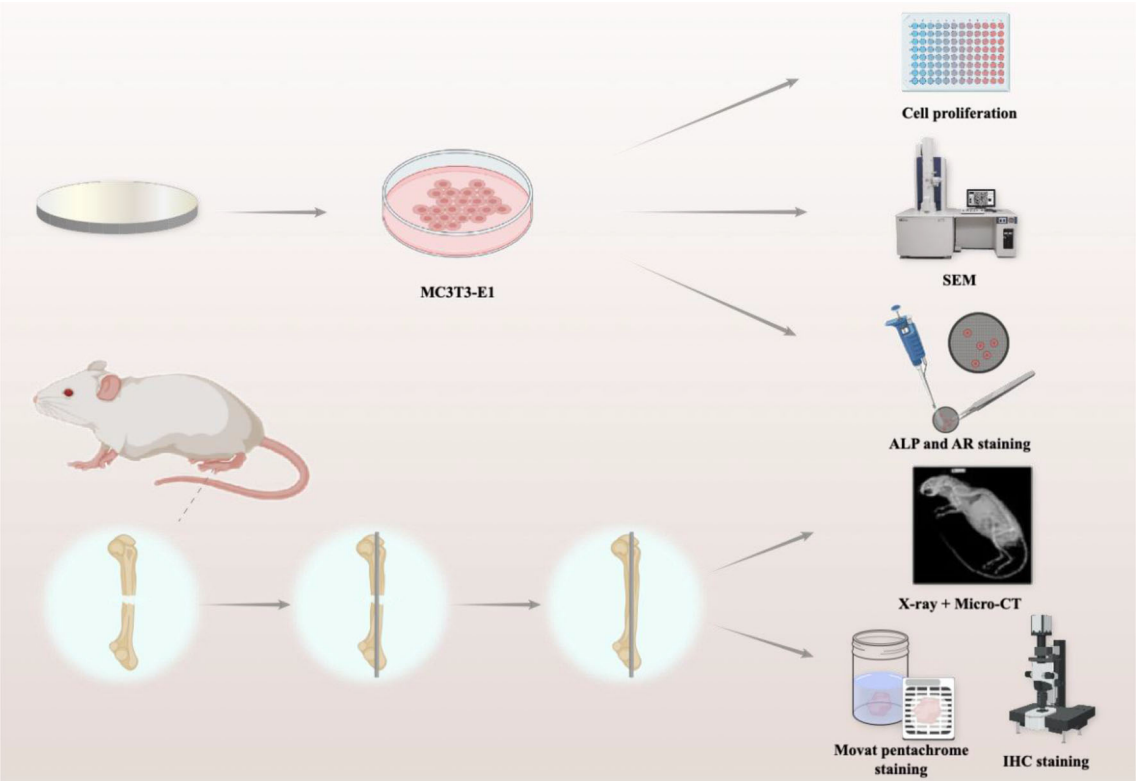

Keywords Fracture healing · Ti45Nb alloy · PI3K–Akt pathway · Orthopedic implant

Introduction

In clinical practice, fractures are one of the common diseases and account for more than billions of dollars in treatment costs, loss of social productivity and personal disability [1]. Fracture healing is a complex coordination of various cellular and mechanosensitive processes, and the outcome of fracture healing depends on many factors, including the severity of trauma, the quality of fracture reduction and fixation (realignment) and comorbidities [2]. Surgical treatment of fractures mainly consists of anatomical reduction and stable fixation, which requires internal fixation devices such as screws, intramedullary nails or plates. Due to their good mechanical properties and biocompatibility, titanium (Ti) implants are widely used in clinical internal fixation instrumentation [3]. Although these implant materials exert excellent mechanical and corrosion resistance properties, there are still some insurmountable disadvantages: (1) the lack of bioactivity and poor osteoconductivity, which makes it difficult to promote fracture healing by regulating osteoblast and osteoclast differentiation, and (2) the local 'stress shielding' effect caused by a high elastic modulus, which is not conducive to osteotylus and bone remodeling [4]. With the development of orthopedic surgical techniques and implant materials, the prognosis of fractures has improved significantly, but a proportion of all fractures still exhibit delayed union and nonunion [5]. The occurrence of fracture-related complications remains a major clinical problem, further increasing the physical pain and financial burden of fracture patients [6]. Thus, overcoming the inherent defects of existing orthopedic endosseous implants and developing a new class of internal fixation materials exert great clinical value and social significance, providing better osteoinductive properties.

In recent years, novel metallic biomaterials with good wear resistance, including tantalum (Ta), zirconium (Zr) and niobium (Nb), have received increasing attention [7]. Nb has been investigated and utilized as an implantable material for its remarkable biocompatibility, mechanical properties and corrosion resistance as well as osteoconductive properties [8]. Nb metals presented good biocompatibility and osteogenesis when implanted in soft and hard tissues of rats [9]. In vitro apatite formation assays and in vivo histomorphometric studies demonstrated that Nb metals are biologically active and can be biologically bonded to bone [10]. In contrast, the

elastic modulus of Ti–Nb alloys is stoichiometrically dependent, and it is lower than 85 GPa when the weight of Nb is between 10% and 20% or between 35% and 50%, which is closer to human bone compared with Ti6Al4V, whose elastic modulus is approximately 114 GPa, thus minimizing the stress shielding effect and additionally combining excellent biocompatibility and corrosion resistance [11, 12]. Chen et al. [13] found that a Ti–Nb alloy facilitates cell adhesion and exhibits significantly enhanced cell–material interactions. Additionally, the nontoxicity of Ti–Nb alloy provides a good basis for its use as a clinical implant material [14, 15]. However, despite the literature illustrating the excellent biocompatibility of Ti–Nb alloys, in vivo studies of Ti–Nb alloys for fracture healing are still lacking, and the mechanism by which Ti–Nb alloys promote fracture healing has not been clarified and remains to be explored.

Our previous studies have suggested that Nb may promote fracture healing by upregulating the PI3K–Akt signaling pathway [16]. The PI3K–Akt signaling pathway is the foundation of various cellular processes, such as cell growth, survival and proliferation. Yang et al. [17] found that extracellular vesicle-encapsulated microRNA-29b-3p could facilitate fracture healing by activating the PI3K–Akt signaling pathway. Dong et al. [18] suggested that the PI3K–Akt and Wnt/β-catenin pathways were closely related to fracture healing. Therefore, we speculated that the Ti–Nb alloy might affect the fracture healing process by stimulating the PI3K–Akt signaling pathway.

In our study, we determined the in vitro cytocompatibility and in vivo biosafety of Ti45Nb alloy and Ti45Nb serving as intramedullary nails in a rat femur fracture model to evaluate its effect on fracture healing compared to Ti6Al4V. Furthermore, histological evaluation and an attempt to explore its main signaling pathways were performed. Therefore, we hypothesized that Ti45Nb alloy has the potential to promote fracture healing, and it presents potential for clinical transformation.

Materials and methods

Sample characterization

The microstructure of the material surface was observed by scanning electron microscopy (SEM, S-4800; Hitachi, Japan). Energy-dispersive spectroscopy (EDS) was performed to detect the elements contained in the materials. Before performing SEM scanning, all samples were coated with platinum (Pt) to increase the electrical conductivity. Ti45Nb was characterized by X-ray diffraction (XRD, Rigaku MiniFlex 600, Cu Ka).

In vitro cytocompatibility and osteogenic differentiation

Cell proliferation and morphology

In in vitro experiments, samples with a round shape and 2 mm height × 10 mm diameter were cocultured with MC3T3-E1 cells at a density of 5×10^4 cells per well on the surface in a 24-well plate. Cells were incubated in alpha minimal essential medium (α-MEM) with 10% fetal bovine serum (FBS) at 37 °C and 5% CO_2. Cell counting kit-8 (CCK-8) (Dojindo Molecular Technology, Japan), following a previous protocol that added reagent into wells at a ratio of 1:10 for 2 h, was used to examine the cell viability, and the cell proliferation rate was detected at 1, 3, 5, and 7 d after coculture with the samples. An ELX800 absorbance zymograph (Bio-Tek, USA) was used to examine the optical density (OD) at 405 nm. MC3T3-E1 cells were incubated in α-MEM with 10% FBS for 7 d. After removal of the medium, each well was washed three times with phosphate-buffered saline (PBS) and then fixed using 4% paraformaldehyde solution for 30 min at 37 °C. Next, each sample was stained with phalloidin for 30 min for cytoskeletal structure staining, and the nuclei were restained with 4',6-diamidino-2-phenylindole (DAPI, Sigma, D9542-10MG) for 15 min. The results were obtained by fluorescence microscopy (Leica Microsystems, Heidelberg, Germany).

Live/dead staining

MC3T3-E1 cells seeded at a density of 5×10^4 cells per well in a 24-well plate were incubated with the material and corresponding medium for 24 h. Then, the cells were stained with a calcein-acetoxymethyl (AM)/propidium iodide (PI) double staining kit (Dojindo Molecular Technology, Japan) to perform a live/dead assay.

Osteogenic differentiation

To investigate the osteogenic differentiation ability of each sample, we performed alkaline phosphatase (ALP) and alizarin red staining. Briefly, MC3T3-E1 cells (5×10^4 cells per well) were cocultured on the surface of Ti6Al4V and Ti45Nb for 3 d. When the cells were completely adherent to the samples, the growth medium was removed and replaced with osteogenic differentiation medium (HUXMA-90021, Cyagen, USA), which was then removed and changed every 3 d. An ALP activity assay kit (P0321; Beyotime, China) was used according to a previous protocol to detect and measure ALP activity at 405 nm. After 21 d of coculture, the samples were transferred to another 24-well cell plate, washed three times with PBS and fixed in 4% paraformaldehyde for 30 min at 37 °C. After alizarin red staining, mineralized nodules were dissolved in 10% cetylpyridinium chloride

(C9002-25G; Sigma, USA) and analyzed semiquantitatively by measuring the absorbance at 562 nm.

Quantitative real-time polymerase chain reaction (RT-PCR)

Total RNA from MC3T3-E1 cells under consistent culture conditions coincubated with the material was extracted according to the TRIzol method. Reverse transcription was conducted on cDNA by PrimeScript RT Master Mix (Takara). RT-PCRs were performed utilizing SYBR Premix Ex TaqII (Takara) on a CFX96 PCR system (Bio Rad). The mRNA expression of osteopontin (OPN), osteocalcin (OCN), ALP, type 1 collagen (Col-1) and runt-related transcription factor-2 (Runx2) was investigated for osteogenic differentiation of MC3T3-E1 cells. Glyceraldehyde-3-phosphate dehydrogenase (GAPDH) served as the housekeeping gene for the control.

Western blot (WB) analysis

On Day 14, cells cocultured with materials were lysed using radio immunoprecipitation assay (RIPA) lysis buffer (P0013K, Beyotime, China) for 30 min at 4 °C. After centrifugation, protein concentrations were detected using a colorimetric assay (Thermo Scientific, MA, USA). Next, loading buffer (P0015, Beyotime, China) was added to the centrifuge tube and then boiled at 100 °C for 10 min. An equal amount of protein was added to the lane for electrophoresis and then transferred to a polyvinylidene fluoride (PVDF) membrane (IPVH00010, Millipore, USA), which was then incubated with 5% skim milk. Anti-Akt (4691 L, Cell Signaling, China), anti-PI3K (ab227204, Abcam, UK), anti-Col-1 (14,695–1-AP, Proteintech, China), anti-ALP (ab108337, Abcam, UK), anti-OCN (ab93876, Abcam, UK) and anti-OPN (22,952–1-AP, Proteintech, China) were incubated overnight at 4 °C, followed by incubation with secondary antibodies for 1 h at 37 °C, and detected using enhanced chemiluminescence (ECL) reagent (Millipore, USA).

Establishment of the animal model

In vivo experiments were conducted in accordance with the Chinese Animal Experimentation Law and approved by the Ethics Committee of Shanghai Jiao Tong University School of Medicine (ethical number: SH9H-2022-A98-1). Eight-week-old male Sprague–Dawley rats (Shanghai Sipper BK Laboratory Animals Ltd., Shanghai, China, n=78) were used for in vivo experiments. The rats were randomly separated into two groups, and anesthesia was completed with an abdominal injection of sodium pentobarbital. The surgical area was shaved and sterilized, and a 2-cm incision was made on the lateral side of the right hind leg to expose the quadriceps muscle by opening the skin and fascial layer, and the femur was revealed by bluntly separating the muscle. A transverse osteotomy was performed at the mid-femur with a reciprocating saw, and the two groups of animals were fixed using niobium and Ti6Al4V rods of 3.5 cm in length and 1.5 mm in diameter as intramedullary nails [19]. The incisions were sutured layer by layer and disinfected again. A sterile calcium xanthophyll solution of 20 mg/kg was injected subcutaneously into the right femur 7 and 14 d before sampling. Sampling was performed after euthanasia of the experimental animals at 4, 8 and 12 weeks after surgery.

Medical imageology evaluation

Anterior posterior (AP) and lateral views of the right femur were determined using a Faxitron MultiFocus X-ray system (Faxitron, Bioptics, LLC, USA) for animals following the manufacturer's instructions. After fixation in 4% paraformaldehyde for 3 d, the femoral specimens were stored in 70% ethanol for micro computed tomography (micro-CT) scanning (μCT 80; SCANCO Medical AG, Bassersdorf, Switzerland). The mid-femur was considered the region of interest. The 200 layers above and below the fracture stacking line were the center, and the layer thickness was 18 μm. A high-resolution three-dimensional (3D) reconstruction of the mid-femur was also performed. Bone volume/tissue volume (BV/TV), mean trabecular thickness (Tb.Th), mean trabecular spacing (Tb.Sp) and trabecular number (Tb.N) were quantitatively analyzed.

Histological analysis

After micro-CT analysis, the samples were embedded in methyl methacrylate (MMA). Hard tissue sections were made from the embedded specimens using the Cut and Grind System (Buehler 11-1280-250, USA). Tissue sections were stained with van Gieson's picrofuchsin. Images were captured by a Nikon SMZ 1500 stereo-zoom microscope (Nikon Instruments, Melville, NY, USA). Femoral specimens were fixed in 4% paraformaldehyde for 72 h and decalcified with ethylenediaminetetraacetic acid. After dehydration, all decalcified femoral specimens were embedded in paraffin. The samples were cut and then further subjected to hematoxylin–eosin (H&E) staining, Movat staining and immunohistochemical staining for PI3K and Akt.

Statistical analysis

Data are presented as the mean±standard deviation. Student's t-test and one-way analysis of variance (ANOVA) were implemented to determine the variance using SPSS version 23.0 software (IBM Corp., Armonk, USA). A P value less than 0.05 was considered to indicate a significant difference.

Results

Materials characterization

The disks used in the in vitro experiment are shown in Fig. 1a. SEM was utilized to examine the characteristics and morphology of Ti45Nb and Ti6Al4V (Fig. 1b). The EDS results showed that no other elements were found in the Ti45Nb disks (Fig. 1c). The XRD results showed that the Ti45Nb alloy mainly shows the β-TiNb phase (Fig. S1 in Supplementary Information).

Cell proliferation and adhesion

Biocompatibility is one of the most important evaluation indices when selecting bone repair materials [14]. Therefore, we first evaluated the adhesion and proliferation of cells after coculture with the material. To investigate cell adhesion, we performed fluorescence staining of MC3T3-E1 cells (Fig. 2a). DAPI and phalloidin staining showed that the amount of cell adhesion in the Ti45Nb group was greater than that in the Ti6Al4V group, and the cells in the Ti45Nb group were more dispersed than those in the Ti6Al4V group. Additionally, a CCK-8 assay was conducted to examine the proliferation rate between the two groups (Fig. 2b), and the results showed that the number of cells in the Ti45Nb and Ti6Al4V groups significantly increased with increasing incubation time. Collectively, this result indicated that Ti45Nb had better in vitro cytocompatibility performance, and the cell number in the Ti45Nb group was similar to that in the control group, which proved that Ti45Nb was nonsignificantly toxic to MC3T3-E1 cells.

Live/dead staining

The results of live/dead staining showed that the number of dead cells in the Ti45Nb group did not significantly increase compared with the Ti6Al4V group, which was in accordance with the results above. Ti45Nb was nontoxic to MC3T3-E1 cells and did not alter the cell morphology (Fig. 2c).

Osteogenic differentiation

MC3T3-E1 cells were cultured in media supplemented with ascorbic acid, β-glycerophosphate and dexamethasone to determine the potential osteogenic effect through ALP staining on Day 7 and alizarin red staining on Day 21. ALP activity was higher in the Ti45Nb group than in the Ti6Al4V group (Fig. 3a), which showed that the Ti45Nb group promoted the osteogenic differentiation of MC3T3-E1 cells. Furthermore, alizarin red staining (Fig. 3b) and semiquantitative analysis (Fig. 3c) showed that calcium nodules were formed in all groups, and the number of calcium nodules was remarkably higher in the Ti45Nb group than in the Ti6Al4V group.

Quantitative real-time polymerase chain reaction

Then, quantitative RT-PCR analysis was conducted to examine the expression of the osteogenic markers OPN, OCN, ALP, Col-1 and Runx2 at Day 14 to investigate osteogenic differentiation. The expression levels of those genes were higher in the Ti45Nb group than in the Ti6Al4V group (Figs. 3d–3h). These results suggested that Ti45Nb presented better performance in inducing osteogenic differentiation of MC3T3-E1 cells.

Western blot

The expression levels of ALP, OCN, OPN, Col-1, Akt, and PI3K proteins were investigated by western blotting (Fig. 4a). Then, the statistical data were calculated by grayscale values/internal parameters. The results confirmed the role of Ti45Nb in promoting the expression of osteogenesis-related proteins (Figs. 4b–4e) and upregulating the key factor in the PI3K–Akt signaling pathway (Figs. 4f–4i).

Animal experiments

Since enhanced osteogenic differentiation in vitro demonstrated that Ti45Nb enhances bone-to-implant osseointegration in vivo, we next evaluated implant performance using a rat femur fracture model.

Radiographic evaluation

Radiographic and micro-CT analyses were conducted to investigate postoperative new bone formation. X-ray results showed that fracture lines were visible in both groups at week 4, with more dense bone forming around the fracture line in the Ti45Nb group than in the Ti6Al4V group (Fig. 5a). At week 8, there was obvious callus formation around the fracture site in both groups. The formation of continuous callus was nearly complete at 8 weeks post-fracture in the Ti45Nb group. At week 12, the bone around the injured site in the Ti45Nb group was significantly calcified. Furthermore, the fracture line of the Ti45Nb group almost disappeared, and the callus remodeling was significantly better than that of the Ti6Al4V group. In addition, to closely observe the healing process of the fracture, we used micro-CT to examine the samples. As shown in the 3D reconstructed results and cross-sectional images (Fig. 5b), the callus in the Ti45Nb group at week 4 postoperatively was larger than that in the Ti6Al4V group. At weeks 8 and 12, the cross-sectional images showed that the callus in the Ti45Nb group had gradually started to shrink and calcify into lamellar bone after remodeling, while

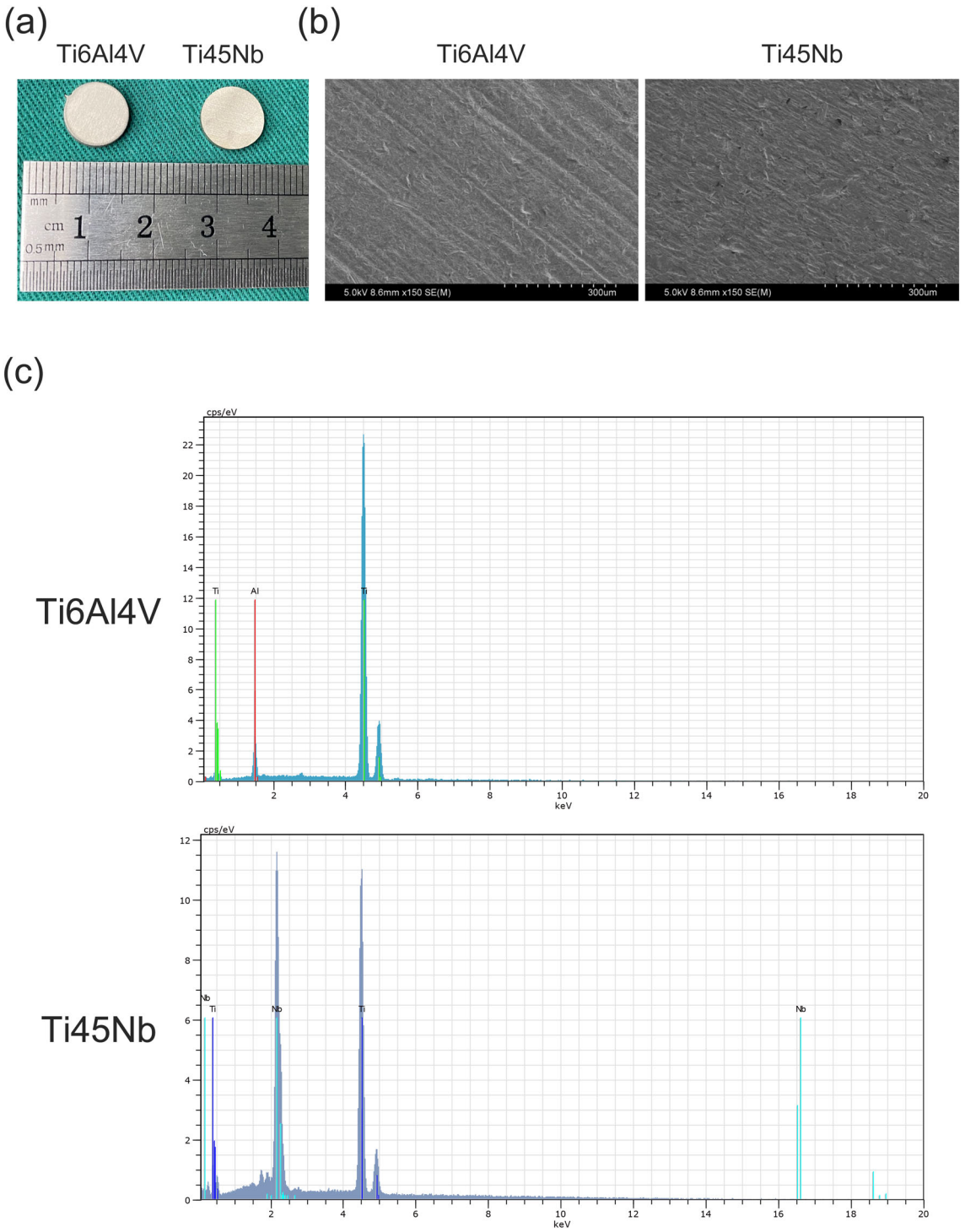

Fig. 1 **a** Ti45Nb and Ti6Al4V disks with a diameter×height of 10 mm×2 mm were used for in vitro experiments. **b** Scanning electron microscopy (SEM) micrographs of the blank disks. **c** Energy-dispersive spectroscopy (EDS) analysis of Ti45Nb and Ti6Al4V disks

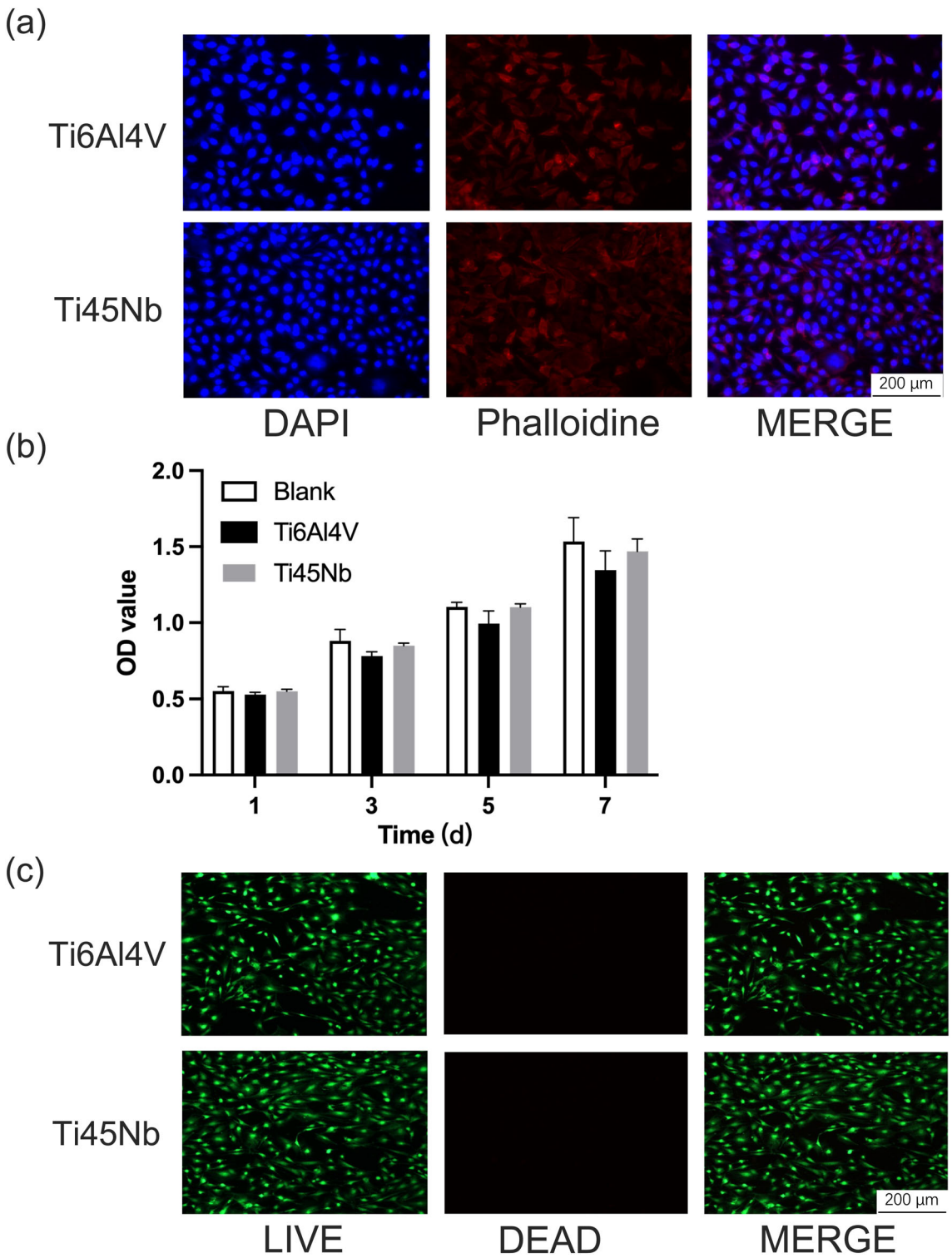

Fig. 2 **a** Fluorescent labeling of MC3T3-E1 cells adhering to the disks. DAPI is presented in blue, and phalloidine is presented in red. **b** Cell growth on Ti45Nb and Ti6Al4V disks at Days 1, 3, 5, and 7, with higher optical density (OD) values indicating more cell growth. Data are presented as mean±standard deviation (n=3). **c** Live/dead staining of MC3T3-E1 cells attached to the disks. DAPI: 4′,6-diamidino-2-phenylindole

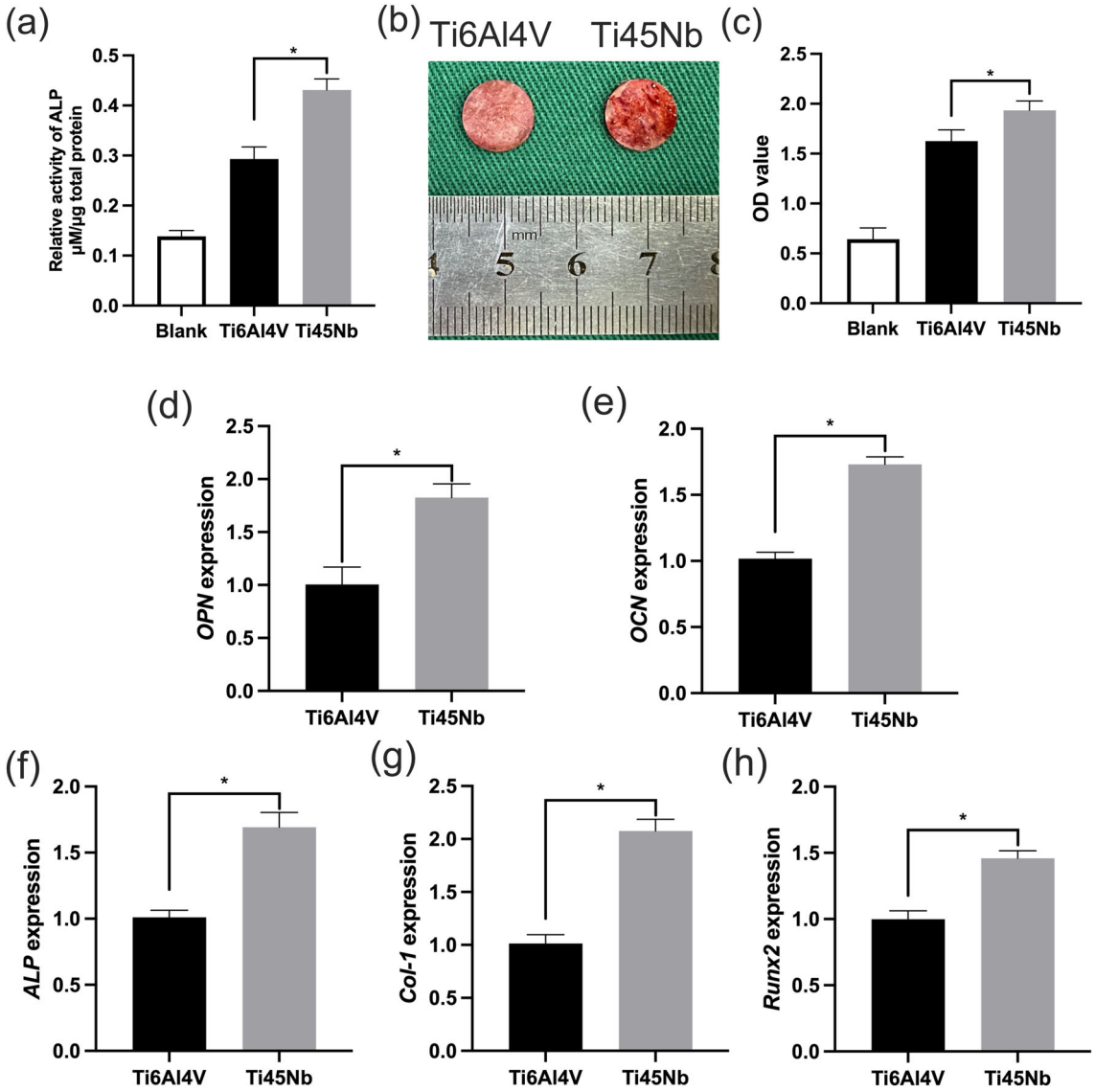

Fig. 3 **a** ALP activity at Day 7. **b** Alizarin red staining of the disks. **c** Semiquantitative analysis of calcium nodules on disks cultured on Day 21, with higher OD values indicating increased formation of calcium nodules in the Ti45Nb group. **d**–**h** Expression of osteogenesis-related genes in the Ti45Nb and Ti6Al4V groups: **d** *OPN*, **e** *OCN*, **f** *ALP*, **g** *Col-1*, and **h** *Runx2*. Data are represented as mean±standard deviation (n=3/group). $^{*}P<0.05$ vs. the Ti6Al4V group. ALP: alkaline phosphatase; OD: optical density; OPN: osteopontin; OCN: osteocalcin; Col-1: type 1 collagen; Runx2: runt-related transcription factor-2

the Ti6Al4V group still showed larger callus tissue. Compared with the Ti6Al4V group, the Ti45Nb group had higher BV/TV values at all time points, and the Ti45Nb group also had the higher number of trabeculae and trabecular thickness and lower trabecular spacing among the two groups at week 12 (Figs. 5c–5f). Overall, Ti45Nb not only promoted osteogenesis but also upregulated remodeling efficiency, resulting in a better recovery of early mechanical stability of the fractured femur.

Histological evaluation

H&E staining showed the general morphology of the callus (Fig. 6a). At week 4 in the Ti6Al4V group, there were mainly fibrous components, while the Ti45Nb group showed more calcified tissue. At week 8, the fibrous healing tissue around the fracture site was completely calcified in the Ti45Nb group. The Ti45Nb group was completely calcified into woven bone, and remodeling and consolidation of the calcified callus occurred. Remodeling of the callus was better in the Ti45Nb group by week 12. Movat staining (Fig. 6b)

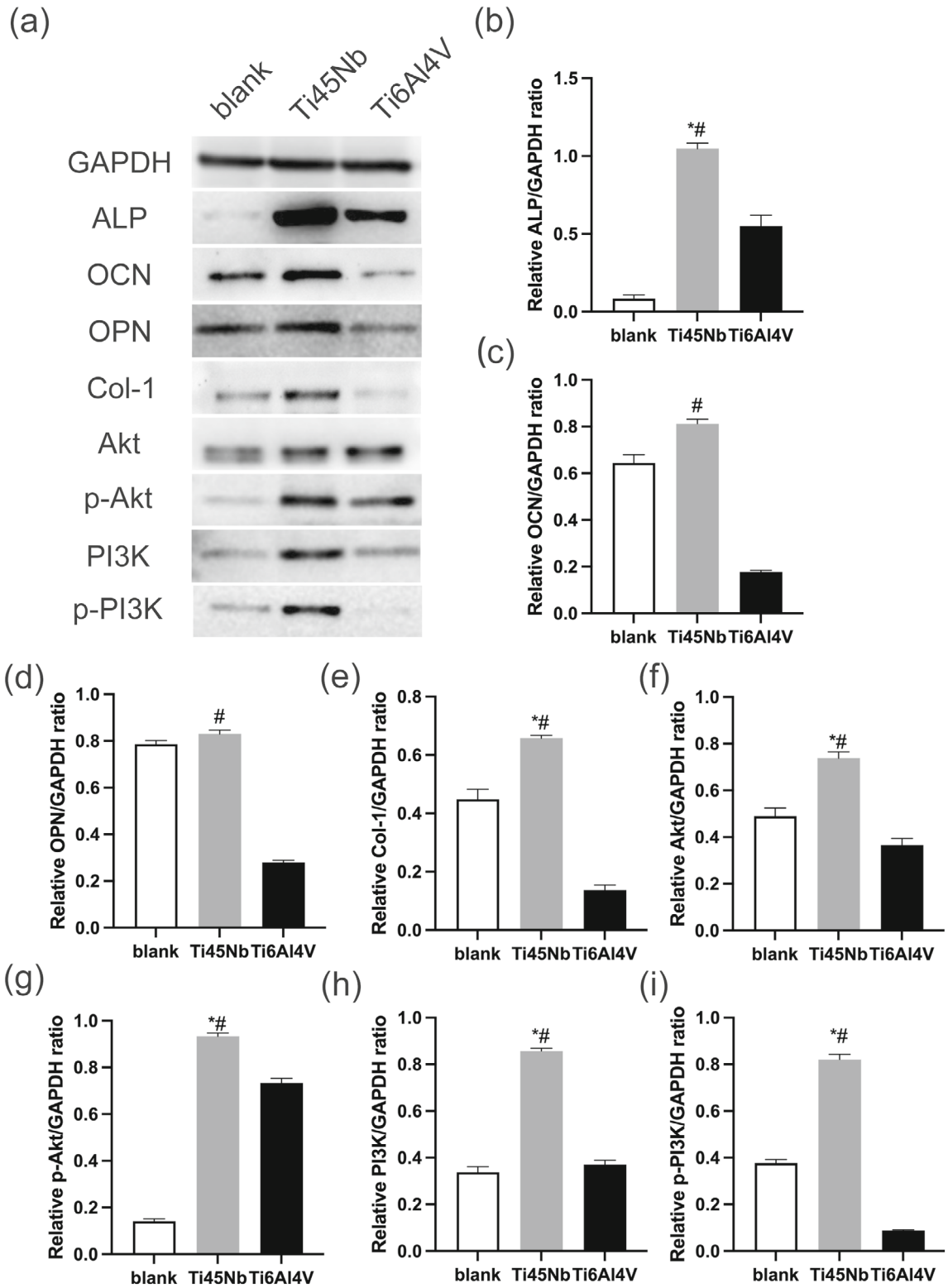

Fig. 4 **a** Western blot analysis of the expression of **b** ALP, **c** OCN, **d** OPN, **e** Col-1, **f** Akt, **g** p-Akt, **h** PI3K, and **i** p-PI3K, relative to GAPDH indicating that Ti45Nb promotes fracture healing correlated with activation of the PI3K/Akt signaling pathway. Data are represented as mean±standard deviation (n=3/group). $^{*}P<0.05$ vs. the blank group; $\#P<0.05$ vs. the Ti6Al4V group. ALP: alkaline phosphatase; OCN: osteocalcin; OPN: osteopontin; Col-1: type 1 collagen; GAPDH: glyceraldehyde-3-phosphate dehydrogenase

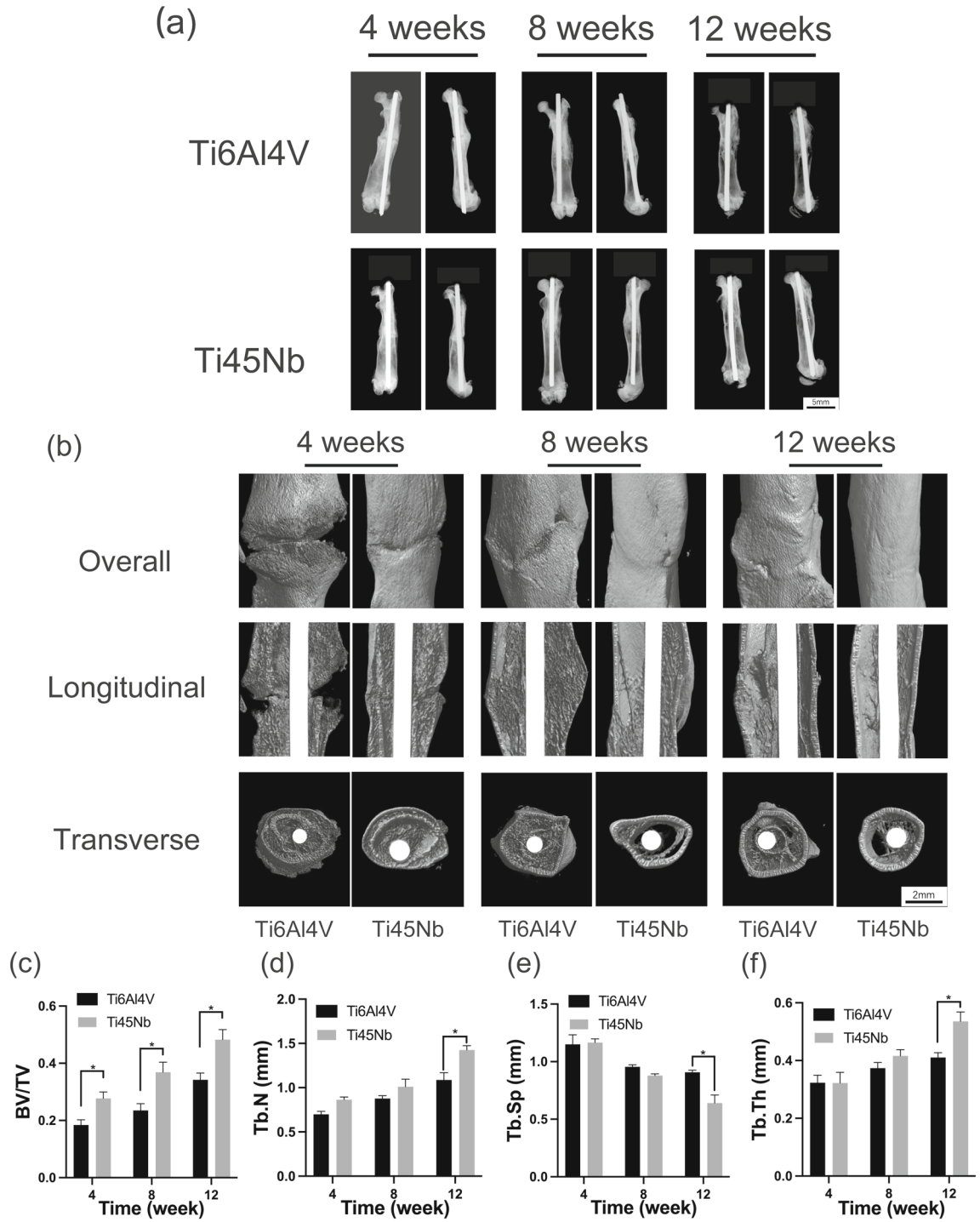

Fig. 5 **a** Radiology analysis using X-ray during follow-up (AP and lateral view). **b** Micro computed tomography (micro-CT) results of the femur. **c** Bone volume/tissue volume (BV/TV) value, **d** trabecular number (Tb.N), **e** trabecular spacing (Tb.Sp) and **f** trabecular thickness (Tb.Th) of the Ti45Nb and Ti6Al4V groups at weeks 4, 8 and 12. Data are represented as mean±standard deviation (n=3/group). $^{*}P<0.05$ vs. the Ti6Al4V group

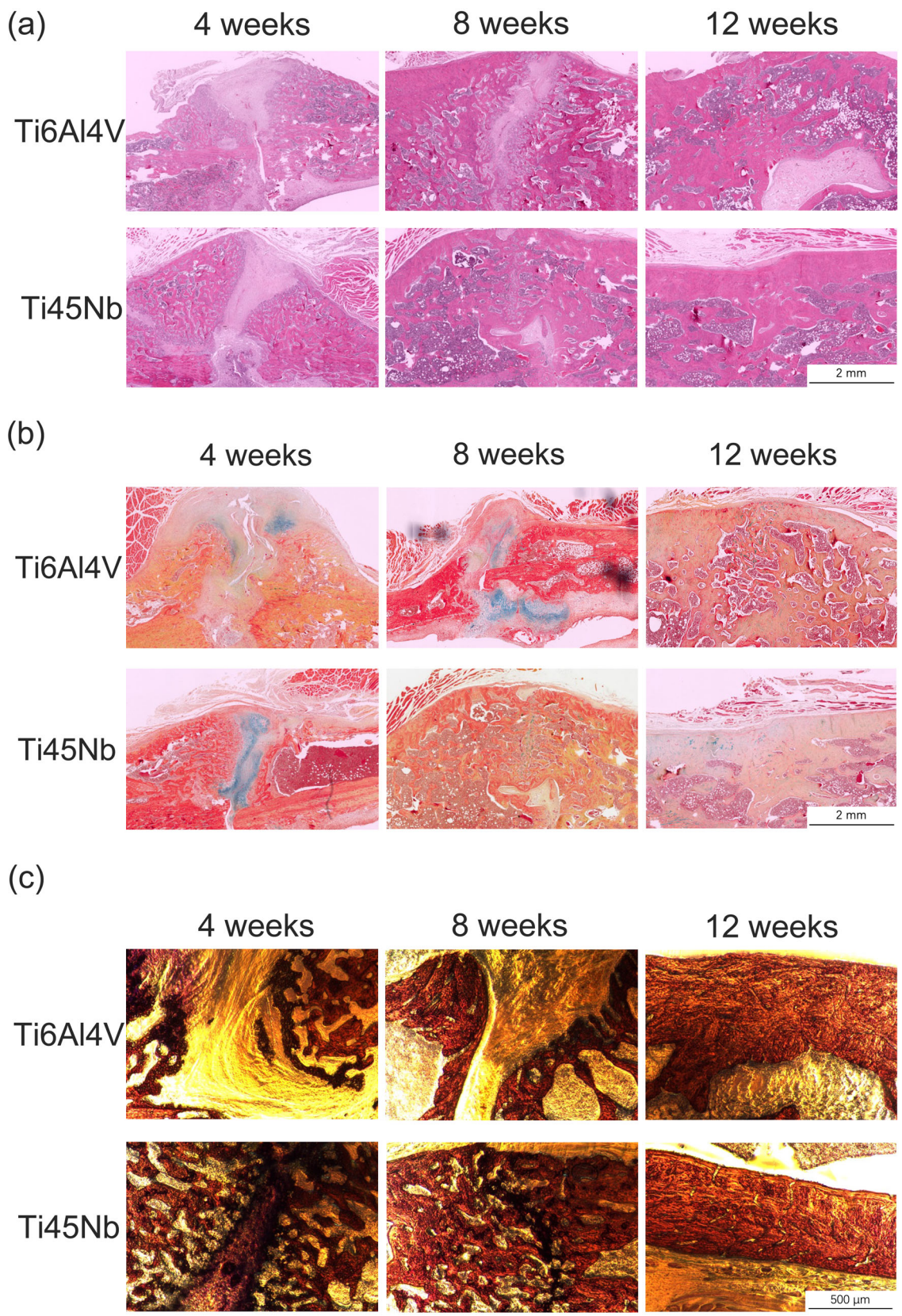

Fig. 6 **a** The results of hematoxylin–eosin (H&E) staining of the fracture sites. **b** Evaluation of the calcification of bone and cartilage using Movat staining. **c** Evaluation of fracture healing via van Gieson staining

showed that the Ti45Nb group had more cartilage calcification at week 4 and had completely calcified into woven bone at week 8, while the Ti6Al4V group showed more cartilage calcification only at week 8. van Gieson staining of both groups at each time point (weeks 4, 8 and 12) is presented in Fig. 6c. Compared with the Ti6Al4V group, the Ti45Nb group had a larger area of new bone at week 8 and a smaller area at week 12. These results suggest that Ti45Nb can accelerate the formation of new bone. During fracture healing, new bone formation and bone reconstruction can be evaluated by continuous fluorescent labeling using calcein. The distance between calcein markers was used to represent the temporal variation in new bone formation or bone remodeling. During the scab formation phase, the greater the distance between calcein markers is, the faster the rate of bone formation is. In this study, at weeks 4 and 8, the distance between calcein markers was farther in the Ti45Nb group than in the Ti6Al4V group, indicating that Ti45Nb induced new bone formation (Fig. S2 in Supplementary Information). At week 12, the distance between calcein markers decreased in both groups, suggesting that bone remodeling was occurring.

Immunohistochemical evaluation

The results of immunofluorescence staining shown in Fig. 7 indicated that the expression of the Ti45Nb group was higher than that of the control group, which suggests that Ti45Nb may accelerate early fracture healing by activating the PI3K–Akt signaling pathway.

Biosafety evaluation

There were no remarkable differences between the body weights of the animals in the Ti45Nb and Ti6Al4V groups (Fig. 8a). Histological analysis was conducted to examine the toxicity of major organs, including the liver, spleen and kidneys. The results were observed using light microscopy, and no significant differences were found between the Ti45Nb and Ti6Al4V groups in the microstructure of the heart, liver, spleen, lung or kidney (Fig. 8b).

Discussion

Fractures are one of the most common injuries of the musculoskeletal system, and when fractures require open reduction and internal fixation surgery, implants are needed to provide better conditions for fracture healing. Therefore, implants must meet the following basic requirements: (1) maintaining their mechanical properties long enough for bone healing, with appropriate mechanical strength [20], (2) good biocompatibility, and (3) being able to promote or at least not impeding bone regeneration and osseointegration [21]. In this study, we first evaluated the biocompatibility and osteogenic differentiation-enabling activity of Ti45Nb alloy in vitro, and the experimental results showed that Ti45Nb has good biocompatibility and osteogenic performance compared to Ti6Al4V, which indicates that Ti45Nb has potential for clinical applications. Next, we established an in vivo rat femur fracture model to investigate the fracture healing ability of Ti45Nb metal as an intramedullary nail compared to the control Ti6Al4V group, which is currently the most commonly used nail.

As a result, we confirmed that Ti45Nb as intramedullary nails could reduce the fracture healing time by promoting early fracture formation. Thus, Ti45Nb-based plates can be an effective means of treating fractures in clinical practice and have good prospects for clinical translation. Currently, the widely used internal fixation devices are mainly made of titanium; however, there are some insurmountable disadvantages of implant materials, including nonbiological activity and implant-associated infection [22, 23]. Thus, the development of implant materials for hard tissues is currently focused on optimizing and enhancing mechanical properties and biocompatibility. Currently, the most common method is to modify the implant surface using bionic coatings to enhance the bioactivity and resistant performance to avoid implant infection, with the expectation of prolonging the life of the implant and reducing the risk of revision surgery. It has been reported that hydroxyapatite (HAp) coatings, with excellent osteoconductivity and bioactivity, are capable of creating a stable interface between the implant and bone, and HAp coatings should have good adhesion and stability to the substrate [24]. However, the main problem with HAp coatings remains the occurrence of delamination with the underlying substrate, and the particles generated by the delamination of the coating can cause inflammatory reactions around the implant [25]. Although it is possible to improve these problems by sol–gel processes, electrophoretic deposition, pulsed laser deposition and electrospray deposition, each of these techniques has its own shortcomings [26].

The way to optimize implants is not only the addition of coatings but also the development of new implant materials, such as tantalum (Ta) metal and its alloys. Tantalum is a bioactive metal with good biocompatibility and corrosion resistance; however, its large elastic modulus and weight are the main reasons that limit its widespread clinical application, and therefore, many researchers have managed to find alternative methods to overcome this challenge. For example, porous Ta scaffolds prepared using 3D printing technology have not only regular pore shape and connectivity but also controlled elastic modulus and compressive strength, which improved osteogenic and osseointegration outcomes in vitro and in vivo compared with porous Ti6Al4V scaffolds [21]. As a novel implant, porous Ta has good biocompatibility, excellent bioactivity, good corrosion resistance and suitable

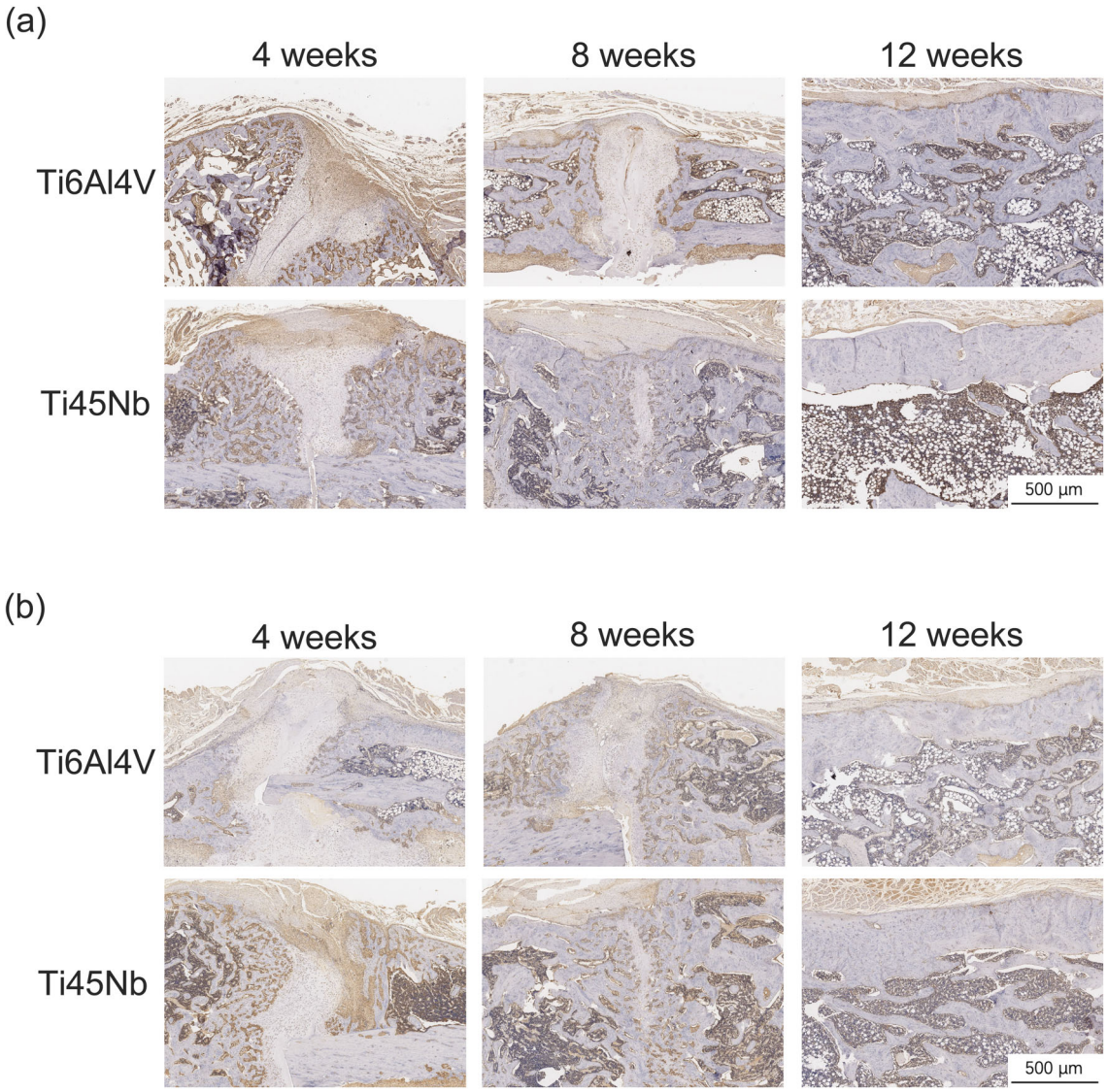

Fig. 7 Immunohistochemical staining of **a** Akt and **b** PI3K

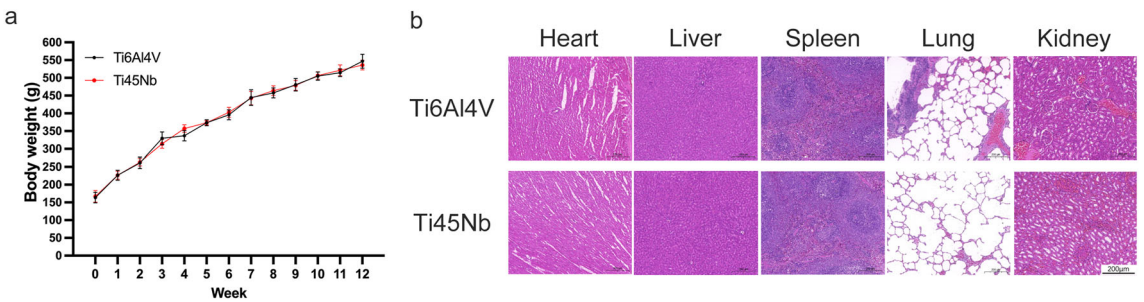

Fig. 8 **a** Body weights of experimental animals in the Ti45Nb and Ti6Al4V groups. **b** The results of hematoxylin–eosin (H&E) staining of the heart, liver, spleen, lung, and kidney assessed (magnification 100×). Data are presented as the mean±standard deviation (n=5)

biomechanical properties, and several Ta-related products have been developed for osteoarticular applications, such as hip and knee arthroplasty and spine surgery [27]. However, there are no uniformly optimized parameters for the inconsistency of parameters in various types of tantalum-containing implants. Although there have been numerous studies on Ti–Ta alloys [28–30], the optimal ratio of Ti–Ta content has not been determined, and new material modification methods need to be developed. In addition, the specific mechanisms of how Ta affects the physicochemical and biological properties have not been elucidated, and the fabrication of porous tantalum scaffolds is complex and costly.

Nb and Ta have similar physical and chemical properties, including excellent biocompatibility, mechanical properties and corrosion resistance as well as osteoconductivity [31]. There have been a number of studies on niobium-based coatings; for example, Nb_2O_5 commonly serves as a protective and enabling bone coating for Ti alloys and stainless steels to improve the biocompatibility and corrosion resistance of implants [32]. The application of Nb-containing alloys in scaffolds has attracted attention. Studies have shown that Ti–Nb alloy has better mechanical properties and biocompatibility than Ti6Al4V [33]. Rao et al. [34] suggested that porous TiNbZr with bioactive nanostructured titanate network coatings could be used for bone tissue engineering. In this study, Ti45Nb promoted MC3T3-E1 cell adherence and osteogenic differentiation compared to Ti6Al4V, presenting remarkable osteogenic potential. Subsequently, we performed an in vivo experiment to determine the effect of Ti45Nb on osteogenesis. In radiology and histological analysis, we observed that the Ti45Nb group exhibited earlier bone formation at week 4 compared to the Ti6Al4V group, and at week 8, the Ti45Nb group showed better bone remodeling than the Ti6Al4V group. At week 12, the Ti45Nb group also showed faster completion of callus remodeling than the control group, indicating that Ti45Nb was able to accelerate fracture healing.

As a representative degradable metal, magnesium alloy has attracted extensive attention from clinicians in the field of orthopedic implants [35, 36]. Moreover, as a bioactive metal, magnesium alloy shows good bone inductivity after implantation, and the degradation products of magnesium can promote fracture healing by regulating bone formation and absorption [37]. Magnesium rods have been shown to be effective in increasing local bone density in animal models [38]. However, the common disadvantages of these magnesium-based implants are an uncontrolled rate of degradation, high hydrogen production, interference with osteoblast migration and isolation of bone tissue, thus affecting bone repair. More importantly, rapid implant degradation is likely to lead to a significant decrease in implant mechanical strength, which may lead to failure of internal fixation.

According to previous studies, there are multiple crucial signaling pathways involved in the fracture healing and repair process, including Wnt/β-catenin, Notch, bone morphogenetic protein (BMP)/transforming growth factor β (TGF-β), etc. Wnt signaling plays an important role in cell proliferation, differentiation, growth, survival, development, regeneration and self-renewal [39]. However, there is some controversy regarding Wnt/β-catenin signaling during different stages of fracture repair in fracture healing models. In the early stage, inhibition or activation of Wnt pathway bone healing affects the differentiation of mesenchymal stem cells (MSCs) into osteoblasts [40]. Notch signaling is involved in controlling the proliferation, differentiation and apoptosis of osteoblasts, osteoclasts, osteocytes and chondrocytes and has a critical role in bone development. BMPs belong to the TGF-β superfamily as multifunctional paracrine growth factors. Additionally, both in vivo and in vitro experiments have demonstrated the significance of the BMP/TGF-β signaling pathway at the onset of bone formation [41]. Moreover, BMP signaling plays a central role in both cartilage formation and osteogenesis [42]. Similarly, the PI3K/Akt pathway plays a crucial role in multiple cellular processes, including cell growth, survival, proliferation and motility [43], and is a key signaling pathway regulating the bone regeneration process in many systems, which can also be considered a key intracellular signaling pathway associated with bone formation [44]. Dong et al. [45] found that an extract of concentrated growth factor activated the PI3K/Akt signaling pathway and promoted osteogenic differentiation and mineralization of MC3T3-E1 cells, thus enhancing osteogenesis in a rat model of cranial defects. A number of studies have reported the key regulatory functions of PI3K signaling and its upstream and downstream targets in bone formation and remodeling. For example, TGF-β also interacts with the PI3K/Akt pathway and promotes osteoconduction during wound healing [46]; BMP-2 promotes osteoblast differentiation by activating the PI3K/Akt pathway [47]. We found higher expression of PI3K and Akt in the Ti45Nb group in histological staining at weeks 4 and 8 and significantly at the callus, indicating a role in the endochondral ossification of the callus. Endochondral ossification is an important process in fracture healing and is induced by BMP, TGF-β2 and TGF-β3 signaling in cartilage healing tissues [48]. At the end of this phase, the formed cartilage calcifies and is replaced by woven bone [49]. Therefore, we speculate that the mechanism by which Ti45Nb promotes fracture healing may involve BMP-induced Akt phosphorylation and the PI3K/Akt signaling pathway. However, there are still some limitations of our study: (1) We did not test the mechanical properties of the samples, although the results of X-ray are convincing, and additionally micro-CT and histochemical results have confirmed the efficacy of the Ti45Nb group in promoting fracture healing, and (2) there is a lack of

in-depth study on the upstream and downstream mechanisms of the PI3K–Akt signaling pathway.

Conclusions

We evaluated the osteogenic properties as well as biocompatibility of Ti45Nb in in vitro and in vivo experiments without any local or systemic toxicity to major organs compared to the control group. We also found that Ti45Nb could promote fracture healing by affecting the PI3K–Akt pathway. Collectively, our results suggest that Ti45Nb implants have potential for future orthopedic applications.

Supplementary Information The online version contains supplementary material available at https://doi.org/10.1007/s42242-023-00250-6.

Acknowledgements This work was supported by the National Natural Science Foundation of China (Nos. 81972058, 81902194 and 82202680), the Science and Technology Commission of Shanghai Municipality (No. 22YF1422900), the Shanghai Municipal Key Clinical Specialty, China (No. shslczdzk06701), the National Facility for Translational Medicine (Shanghai), China (No. TMSZ-2020-207), the Shanghai Engineering Research Center of Orthopedic Innovative Instruments and Personalized Medicine Instruments and Personalized Medicine (No. 19DZ2250200) and the Key R&D Program of Ningxia, China (Nos. 2020BCH01001 and 2021BEG02037).

Author contributions JT was involved in conceptualization, investigation, formal analysis and writing—original draft. JXL was involved in investigation, formal analysis and writing—original draft. ZYR and JXW were involved in investigation and formal analysis. DHL and BJC were involved in formal analysis. LD, XPL, and WBJ were involved in methodology. KX was involved in conceptualization, methodology, supervision and writing—review and editing. LW was involved in methodology, supervision and writing—review and editing. YQH was involved in conceptualization, supervision, funding acquisition and writing—review and editing.

Declarations

Conflict of interest The authors declare that they have no conflict of interest.

Ethical approval All institutional and national guidelines for the care and use of laboratory animals were followed. In vivo experiments were conducted in accordance with the Chinese Animal Experimentation Law and approved by the Ethics Committee of Shanghai Jiao Tong University School of Medicine (ethical number: SH9H-2022-A98-1).

References

1. Ghiasi MS, Chen J, Vaziri A et al (2017) Bone fracture healing in mechanobiological modeling: a review of principles and methods. Bone Rep 6:87–100. https://doi.org/10.1016/j.bonr.2017.03.002
2. Claes L, Recknagel S, Ignatius A (2012) Fracture healing under healthy and inflammatory conditions. Nat Rev Rheumatol 8(3):133–143. https://doi.org/10.1038/nrrheum.2012.1
3. Xie K, Zhou Z, Guo Y et al (2019) Long-term prevention of bacterial infection and enhanced osteoinductivity of a hybrid coating with selective silver toxicity. Adv Healthc Mater 8(5):e1801465. https://doi.org/10.1002/adhm.201801465
4. Xie K, Wang L, Guo Y et al (2021) Effectiveness and safety of biodegradable Mg-Nd-Zn-Zr alloy screws for the treatment of medial malleolar fractures. J Orthop Translat 27:96–100. https://doi.org/10.1016/j.jot.2020.11.007
5. Wang L, Li GY, Ren L et al (2017) Nano-copper-bearing stainless steel promotes fracture healing by accelerating the callus evolution process. Int J Nanomed 12:8443–8457. https://doi.org/10.2147/IJN.S146866
6. Metsemakers WJ, Moriarty TF, Nijs S et al (2016) Influence of implant properties and local delivery systems on the outcome in operative fracture care. Injury 47(3):595–604. https://doi.org/10.1016/j.injury.2016.01.019
7. Balla VK, Bodhak S, Bose S et al (2010) Porous tantalum structures for bone implants: fabrication, mechanical and in vitro biological properties. Acta Biomater 6(8):3349–3359. https://doi.org/10.1016/j.actbio.2010.01.046
8. Xu ZJ, Yate L, Qiu Y et al (2019) Potential of niobium-based thin films as a protective and osteogenic coating for dental implants: the role of the nonmetal elements. Mater Sci Eng C Mater Biol Appl 96:166–175. https://doi.org/10.1016/j.msec.2018.10.091
9. Matsuno H, Yokoyama A, Watari F et al (2001) Biocompatibility and osteogenesis of refractory metal implants, titanium, hafnium, niobium, tantalum and rhenium. Biomaterials 22(11):1253–1262. https://doi.org/10.1016/S0142-9612(00)00275-1
10. Wang XJ, Li YC, Lin JG et al (2008) In vitro bioactivity evaluation of titanium and niobium metals with different surface morphologies. Acta Biomater 4(5):1530–1535. https://doi.org/10.1016/j.actbio.2008.04.005
11. Panigrahi A, Bönisch M, Waitz T et al (2015) Phase transformations and mechanical properties of biocompatible Ti–16.1Nb processed by severe plastic deformation. J Alloy Compound 628:434–441. https://doi.org/10.1016/j.jallcom.2014.12.159
12. do Prado RF, Rabelo SB, de Andrade DP et al (2015) Porous titanium and Ti-35Nb alloy: effects on gene expression of osteoblastic cells derived from human alveolar bone. J Mater Sci Mater Med 26(11):259. https://doi.org/10.1007/s10856-015-5594-0
13. Chen YH, Han PP, Dehghan-Manshadi A et al (2020) Sintering and biocompatibility of blended elemental Ti-xNb alloys. J Mech Behav Biomed Mater 104:103691. https://doi.org/10.1016/j.jmbbm.2020.103691
14. Jirka I, Vandrovcová M, Frank O et al (2013) On the role of Nb-related sites of an oxidized β-TiNb alloy surface in its interaction with osteoblast-like MG-63 cells. Mater Sci Eng C Mater Biol Appl 33(3):1636–1645. https://doi.org/10.1016/j.msec.2012.12.073
15. Fischer M, Laheurte P, Acquier P et al (2017) Synthesis and characterization of Ti-27.5Nb alloy made by CLAD® additive manufacturing process for biomedical applications. Mater Sci Eng C

Mater Biol Appl 75:341–348. https://doi.org/10.1016/j.msec.2017.02.060
16. Tan J, Li JX, Cao BJ et al (2022) Niobium promotes fracture healing in rats by regulating the PI3K-Akt signalling pathway: an in vivo and in vitro study. J Orthop Translat 37:113–125. https://doi.org/10.1016/j.jot.2022.08.007
17. Yang JZ, Gao J, Gao F et al (2022) Extracellular vesicles-encapsulated microRNA-29b-3p from bone marrow-derived mesenchymal stem cells promotes fracture healing via modulation of the PTEN/PI3K/AKT axis. Exp Cell Res 412(2):113026. https://doi.org/10.1016/j.yexcr.2022.113026
18. Dong J, Xu XQ, Zhang QY et al (2020) The PI3K/AKT pathway promotes fracture healing through its crosstalk with Wnt/beta-catenin. Exp Cell Res 394(1):112137. https://doi.org/10.1016/j.yexcr.2020.112137
19. Li GY, Wang L, Jiang YH et al (2017) Upregulation of Akt signaling enhances femoral fracture healing by accelerating atrophic quadriceps recovery. Biochim Biophys Acta Mol Basis Dis 11:2848–2861. https://doi.org/10.1016/j.bbadis.2017.07.036
20. Iglesias C, Bodelon OG, Montoya R et al (2015) Fracture bone healing and biodegradation of AZ31 implant in rats. Biomed Mater 10(2):025008. https://doi.org/10.1088/1748-6041/10/2/025008
21. Guo Y, Xie K, Jiang WB et al (2019) In vitro and in vivo study of 3D-printed porous tantalum scaffolds for repairing bone defects. ACS Biomater Sci Eng 5(2):1123–1133. https://doi.org/10.1021/acsbiomaterials.8b01094
22. Hayes JS, Richards RG (2010) The use of titanium and stainless steel in fracture fixation. Expert Rev Med Devices 7(6):843–853. https://doi.org/10.1586/erd.10.53
23. Darouiche RO (2004) Treatment of infections associated with surgical implants. N Engl J Med 350(14):1422–1429. https://doi.org/10.1056/NEJMra035415
24. Lakstein D, Kopelovitch W, Barkay Z et al (2009) Enhanced osseointegration of grit-blasted, NaOH-treated and electrochemically hydroxyapatite-coated Ti-6Al-4V implants in rabbits. Acta Biomater 5(6):2258–2269. https://doi.org/10.1016/j.actbio.2009.01.033
25. Ramaswamy Y, Wu CT, Zreiqat H (2009) Orthopedic coating materials: considerations and applications. Expert Rev Med Devices 6(4):423–430. https://doi.org/10.1586/erd.09.17
26. de Jonge LT, Leeuwenburgh SC, Wolke JG et al (2008) Organic-inorganic surface modifications for titanium implant surfaces. Pharm Res 25(10):2357–2369. https://doi.org/10.1007/s11095-008-9617-0
27. Han Q, Wang CY, Chen H et al (2019) Porous tantalum and titanium in orthopedics: a review. ACS Biomater Sci Eng 5(11):5798–5824. https://doi.org/10.1021/acsbiomaterials.9b00493
28. Ghouse S, Babu S, Nai K et al (2018) The influence of laser parameters, scanning strategies and material on the fatigue strength of a stochastic porous structure. Addit Manuf 22:290–301. https://doi.org/10.1016/j.addma.2018.05.024
29. Leong SS, Edith WF, Yee YW (2018) Selective laser melting of titanium alloy with 50 wt% tantalum: effect of laser process parameters on part quality. Int J Refract Metal Hard Mater 77:120–127. https://doi.org/10.1016/j.ijrmhm.2018.08.006
30. Xia Y, Fang ZZ, Sun P et al (2018) Novel method for making biomedical segregation-free Ti-30Ta alloy spherical powder for additive manufacturing. JOM Metal Mater Society 70(3):364–369. https://doi.org/10.1007/s11837-017-2713-z
31. Zhang S, Cheng X, Yao Y et al (2015) Porous niobium coatings fabricated with selective laser melting on titanium substrates: preparation, characterization, and cell behavior. Mater Sci Eng C Mater Biol Appl 53:50–59. https://doi.org/10.1016/j.msec.2015.04.005
32. Dinu M, Braic L, Padmanabhan SC et al (2020) Characterization of electron beam deposited Nb_2O_5 coatings for biomedical applications. J Mech Behav Biomed Mater 103:103582. https://doi.org/10.1016/j.jmbbm.2019.103582
33. Weinmann M, Schnitter C, Stenzel M et al (2018) Development of bio-compatible refractory Ti/Nb(/Ta) alloys for application in patient-specific orthopaedic implants. Int J Refract Metal Hard Mater 75:126–136. https://doi.org/10.1016/j.ijrmhm.2018.03.018
34. Rao X, Yang JH, Li J et al (2018) Replication and bioactivation of Ti-based alloy scaffold macroscopically identical to cancellous bone from polymeric template with TiNbZr powders. J Mech Behav Biomed Mater 88:296–304. https://doi.org/10.1016/j.jmbbm.2018.08.031
35. Staiger MP, Pietak AM, Huadmai J et al (2006) Magnesium and its alloys as orthopedic biomaterials: a review. Biomaterials 27(9):1728–1734. https://doi.org/10.1016/j.biomaterials.2005.10.003
36. Shuai CJ, Wang B, Yang YW et al (2019) 3D honeycomb nanostructure-encapsulated magnesium alloys with superior corrosion resistance and mechanical properties. Compos B Eng 162:611–620. https://doi.org/10.1016/j.compositesb.2019.01.031
37. Zhang Y, Xu J, Ye CR et al (2016) Implant-derived magnesium induces local neuronal production of CGRP to improve bone-fracture healing in rats. Nat Med 22(10):1160–1169. https://doi.org/10.1038/nm.4162
38. Yang WL, Zhang Y, Yang JH et al (2011) Potential antiosteoporosis effect of biodegradable magnesium implanted in STZ-induced diabetic rats. J Biomed Mater Res A 99A(3):386–394. https://doi.org/10.1002/jbm.a.33201
39. Shi J, Chi SH, Xue J et al (2016) Emerging role and therapeutic implication of Wnt signaling pathways in autoimmune diseases. J Immunol Res 2016:9392132. https://doi.org/10.1155/2016/9392132
40. Krishnan V, Bryant HU, Macdougald OA (2006) Regulation of bone mass by Wnt signaling. J Clin Invest 116(5):1202–1209. https://doi.org/10.1172/JCI28551
41. Zieba JT, Chen YT, Lee BH et al (2020) Notch signaling in skeletal development, homeostasis and pathogenesis. Biomolecules 10(2):332. https://doi.org/10.3390/biom10020332
42. Chijimatsu R, Saito T (2019) Mechanisms of synovial joint and articular cartilage development. Cell Mol Life Sci 76(20):3939–3952
43. Martini M, De Santis MC, Braccini L et al (2014) PI3K/AKT signaling pathway and cancer: an updated review. Ann Med 46(6):372–383. https://doi.org/10.3109/07853890.2014.912836
44. Wang T, Zhang XP, Bikle DD (2017) Osteogenic differentiation of periosteal cells during fracture healing. J Cell Physiol 232(5):913–921. https://doi.org/10.1002/jcp.25641
45. Dong K, Zhou WJ, Liu ZH et al (2021) The extract of concentrated growth factor enhances osteogenic activity of osteoblast through PI3K/AKT pathway and promotes bone regeneration in vivo. Int J Implant Dent 7(1):70. https://doi.org/10.1186/s40729-021-00357-4
46. Zhang ZD, Zhang XZ, Zhao DW et al (2019) TGF-β1 promotes the osteoinduction of human osteoblasts via the PI3K/AKT/mTOR/S6K1 signalling pathway. Mol Med Rep 49(5):3505–3518. https://doi.org/10.3892/mmr.2019.10051
47. Barneda-Zahonero B, Miñano-Molina A, Badiola N et al (2009) Bone morphogenetic protein-6 promotes cerebellar granule neurons survival by activation of the MEK/ERK/CREB pathway. Mol Biol Cell 20(24):5051–5063. https://doi.org/10.1091/mbc.e09-05-0424

48. Gerstenfeld LC, Cullinane DM, Barnes GL et al (2003) Fracture healing as a post-natal developmental process: molecular, spatial, and temporal aspects of its regulation. J Cell Biochem 88(5):873–884. https://doi.org/10.1002/jcb.10435

49. Fayaz HC, Giannoudis PV, Vrahas MS et al (2011) The role of stem cells in fracture healing and nonunion. Int Orthop 35(11):1587–1597. https://doi.org/10.1007/s00264-011-1338-z